DOI: 10.1002/ejic.200800564

Thermal and Catalytic Dehydrogenation of the Guanidine–Borane Adducts $H_3B{\cdot}$hppH (hppH = 1,3,4,6,7,8-hexahydro-2*H*-pyrimido[1,2-*a*]pyrimidine) and $H_3B{\cdot}N(H)C(NMe_2)_2$: A Combined Experimental and Quantum Chemical Study

Oxana Ciobanu,[a] Fayçal Allouti,[a] Pascal Roquette,[a] Simone Leingang,[a] Markus Enders,[a] Hubert Wadepohl,[a] and Hans-Jörg Himmel*[a]

Keywords: Dehydrogenation / Homogeneous catalysis / Heterogeneous catalysis / Hydrogen / Boron / Density functional calculations

Herein thermal and catalytic dehydrogenation of the guanidine–borane adducts $H_3B{\cdot}$hppH (hppH = 1,3,4,6,7,8-hexahydro-2*H*-pyrimido[1,2-*a*]pyrimidine) and $H_3B{\cdot}N(H)C(NMe_2)_2$ are analysed. Thermal decomposition of $H_3B{\cdot}$hppH at 80 °C leads to $[HB(\mu\text{-hpp})]_2$ and a second boron hydride, which is tentatively identified as $[(\kappa^2N\text{-hpp})BH_2]$. Decomposition in boiling toluene (110 °C) leads to a mixture of $[H_2B(\mu\text{-hpp})]_2$ and $[HB(\mu\text{-hpp})]_2$, from which $[H_2B(\mu\text{-hpp})]_2$ can be separated and crystallised. In the presence of a catalyst (with Cp_2TiCl_2/*n*BuLi or $[Rh(1,5\text{-cod})Cl]_2$ as precatalysts) dehydrogenation at 80 °C leads predominantly to $[H_2B(\mu\text{-hpp})]_2$. In the case of $H_3B{\cdot}N(H)C(NMe_2)_2$ uncatalysed dehydrogenation turns out to be a very slow process even at 110 °C. Interestingly, the ultimate product of this process is oligomeric methylimino borane, $[HBNMe]_n$. This pathway can be modelled and understood with the aid of quantum chemical calculations. Faster dehydrogenation can be initiated by addition of a catalyst. Finally, the possible mechanisms for thermal and Cp_2Ti-catalysed dehydrogenation are analysed for the model compound $H_3B{\cdot}N(H)C(NH_2)_2$ by means of quantum chemical (DFT) calculations.

Introduction

Interest in the well-known compound ammonia–borane (AB) was refreshed since the compound was suggested as a hydrogen storage material for mobile applications.[1] In the search for ways to speed up H_2 delivery, the transition-metal-catalysed dehydrogenation of AB was studied experimentally in some depth.[2] Thus, late-transition-metal complexes such as the chloro-(1,5-cyclooctadiene)rhodium(I) dimer, $[Rh(1,5\text{-cod})Cl]_2$, were found to catalyse dehydrogenation of AB.[3] With the catalyst $[(pocop)Ir(H)_2]$ [pocop = 1,3-$(OPtBu_2)_2C_6H_3$],[4] one equivalent of H_2 is obtained from AB in a few minutes at room temperature. Very recently, Fe nanoparticles were prepared and shown to catalyse fast hydrolytic dehydrogenation of AB.[5] Early transition-metal complexes were also studied. Whereas Ti^{IV} species such as Cp_2TiMe_2 are not catalytically active,[3a] a mixture of Cp_2TiCl_2 and *n*BuLi, which most likely contains the intermediate Ti^{II} species Cp_2Ti at temperatures exceeding –50 °C,[6] initiates dehydrogenation of the AB derivative $H_3B{\cdot}NMe_2H$ at 20 °C.[7] Whereas catalysis with Cp_2TiCl_2/*n*BuLi shows all signs of a homogeneous process, Rh clusters and/or nanoparticles are the active species in Rh catalysis.[8] Quantum chemical calculations on the $TiCp_2$-catalysed dehydrogenation of $H_3B{\cdot}NMe_2H$ predict an intramolecular, stepwise mechanism.[9] Very recently, it was shown that this dehydrogenation can also be initiated by acids.[10] Although the accumulated data show that fast dehydrogenation can be achieved, the major obstacle for technology based on AB is that no economically reasonable way has yet been found to recycle the dehydrogenation products.[1]

In the past we synthesised the first representatives of a new class of boron and gallium hydrides that are amenable to dehydrogenation reactions. For this class of compounds, dehydrogenation causes dimerisation and formation of a direct E–E (E = B or Ga) bond [see Equation (1)]. Hence, we already showed that thermally induced dehydrogenation of $H_3B{\cdot}$hppH (**1**) (hppH = 1,3,4,6,7,8-hexahydro-2*H*-pyrimido[1,2-*a*]pyrimidine, see Scheme 1)[11] leads to $[HB(\mu\text{-hpp})]_2$ with a rooftop-type structure. Some related molecules with similar structures were subsequently synthesised in our group (namely, $[(Me_2N)B(\mu\text{-hpp})]_2$, the monocations $[(Me_2HN)B(\mu\text{-hpp})BCl]^+$ and $[(Me_2HN)B(\mu\text{-hpp})_2B(NMe_2)]^+$[12] and the dication $[(Me_2HN)B(\mu\text{-hpp})]_2^{2+}$[13])

[a] Anorganisch-Chemisches Institut, Ruprecht-Karls-Universität Heidelberg,
Im Neuenheimer Feld 270, 69120 Heidelberg, Germany
Fax: +49-6221-545707
E-mail: hans-jorg.himmel@aci.uni-heidelberg.de

Supporting information for this article is available on the WWW under http://www.eurjic.org or from the author.

showing the tendency of the hpp^- ligand to form such dinuclear complexes. Additional work in our group was concerned with other guanidine adducts such as $H_3B{\cdot}N(H)C(NMe_2)_2$ (**2**; see Scheme 1)[14] and the comparison of bonding in guanidine and amine group 13 element hydride adducts.

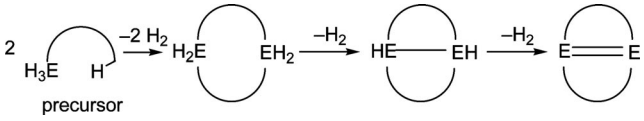

(1)

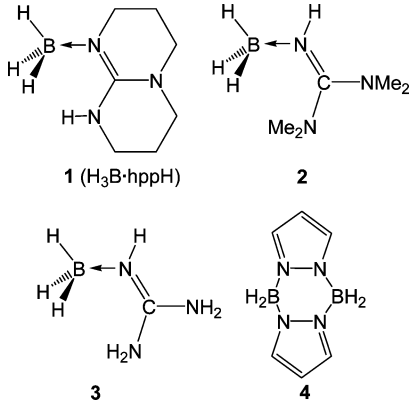

Scheme 1.

Herein we analyse dehydrogenation in the absence and presence of a catalyst and compare catalysed and noncatalysed dehydrogenation of **1** and **2**. Although a comparison with dehydrogenation of AB and derivatives is interesting, it has to be stressed that it is not the intention of this article to propose these two compounds for hydrogen storage. In the course of our studies we succeeded in isolating and structurally characterising with X-ray diffraction the elusive $[H_2B(\mu\text{-hpp})]_2$ molecule (**1c**; Scheme 2). In addition to the experimental work, quantum chemical calculations were carried out on the simple model guanidine complex $H_3B{\cdot}N(H)C(NH_2)_2$ (**3**; Scheme 1), to shed light on the possible reaction mechanisms for the thermal and the Cp_2TiCl_2/*n*BuLi catalysed reaction. In these calculations we followed the idea of an intramolecular, stepwise mechanism that was found to be favoured in the case of $H_3B{\cdot}NMe_2H$.[9] Two possible pathways were considered for thermal and catalytic dehydrogenation leading either to the allene-like $H_2BNC(NH_2)_2$ or to the diene-type $H_2BN(H)C(NH)(NH_2)$, which subsequently dimerises. In addition, the first steps of a thermal dehydrogenation process including isomerisation and decomposition to give amino and imino borane oligomers is considered. The experimental results will prove this pathway to be of importance.

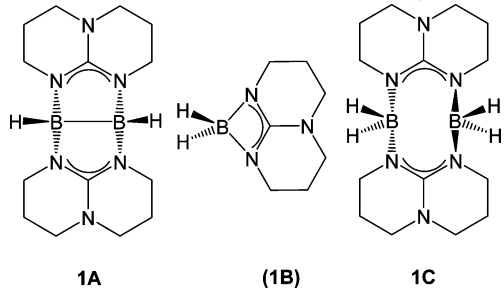

Scheme 2.

Results and Discussion

This section is divided into two parts. We start with an analysis of the mechanism for thermal and Cp_2TiCl_2/*n*BuLi catalysed dehydrogenation of model compound **3** on the basis of quantum chemical calculations. It will be shown that these calculations help to understand the differences in the dehydrogenation reactions between guanidine–boranes and AB or derivatives. Afterwards we discuss the experimental results obtained for compounds **1** and **2**.

Quantum Chemical (B3LYP) Calculations

The catalytic dehydrogenation of $H_3B{\cdot}NMe_2H$ with Cp_2Ti (formed in situ from Cp_2TiCl_2 and *n*BuLi) has been shown to be homogeneous, whereas that with $[Rh(1,5\text{-cod})Cl]_2$ is heterogeneous (or at least involves Rh clusters). Our experimental results argue for a similar situation in the case of the guanidine–boranes. This makes the Cp_2Ti-catalysed reaction a much easier system for calculations. In these calculations we used the same method as in the recently published theoretical work on dehydrogenation of $H_3B{\cdot}NMe_2H$.[9] However, we slightly modified the basis set. The calculations were restricted to a step-by-step model that does not consider the involvement of a second guanidine molecule in the hydrogen elimination. In the case of $H_3B{\cdot}NMe_2H$, it was shown that such a step-by-step mechanism is favoured kinetically over other possibilities. Even with this restriction, we had to consider two possible pathways (in difference to the $H_3B{\cdot}NMe_2H$ case where only one pathway is possible). If the N atom from which H is eliminated is directly bound to B, being thus the imine N atom, the process is named 1,2-dehydrogenation and leads to the allene-type species $H_2BNC(NH_2)_2$. If it is one of the N atoms of the two amido (NH_2) groups, the process is named 1,4-dehydrogenation and results in the diene-type species $H_2BN(H)C(NH_2)(NH)$. In the case of **1**, only 1,4 dehydrogenation is possible, and for **2** only 1,2-dehydrogenation is possible. Therefore, these two molecules are ideal systems to experimentally verify the theoretical results.

Uncatalysed Reaction

We first calculated the possible mechanism for the uncatalysed reactions. An H–H bond is formed at the expense of B–H and N–H bonds in the course of dehydrogenation. To

compare the results with the catalytic reactions, we assumed a mechanism in which the first H_2 molecule is eliminated in an intramolecular process. The structures of the products and the transition states for all considered pathways are illustrated in Figure 1. Table 1 includes calculated thermodynamic properties. Thermally induced 1,4-dehydrogenation of **3** to give $H_2BN(H)C(NH_2)NH$ in its diene-type structure is associated with an energy change of 48.3 kJ mol^{-1}. $\Delta_{solv}G^0$ including solvent effects amounts to not more than +7.0 kJ mol^{-1}. These values are in good agreement to previous calculations.[15] However, a standard Gibbs free energy barrier (including solvent effects) of 109.2 kJ mol^{-1} (at 298 K, 1 bar) opposes dehydrogenation. The H–H bond length in the transition state measures 84.6 pm (compared to 74.4 pm in free H_2). In the diene-type product the B–N bond length (141.1 pm) is significantly shorter than that in the adduct (159.9 pm). At the transition state, the B–N bond length measures 149.9 pm and is thus already significantly strengthened.

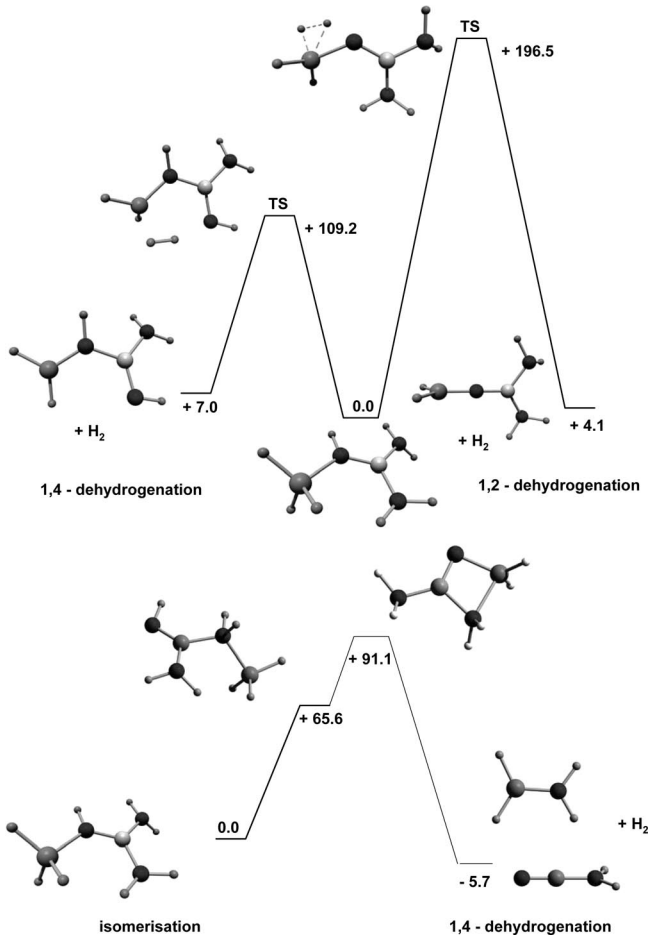

Figure 1. Calculated structures and $\Delta_{solv}G$ for thermal 1,2- or 1,4-dehydrogenation and isomerisation and decomposition under H_2 elimination starting with **3**.

The 1,2-dehydrogenation of **3** is associated with a change in energy and standard Gibbs free energy (including solvent effects) of 43.6 and 4.1 kJ mol^{-1}, respectively. A standard Gibbs free energy barrier as high as 197 kJ mol^{-1} separates the reactant from the product. The transition state features an H–H bond length of 101.2 pm. Again, the B–N bond length in the allene-type product (136.5 pm) is much shorter than that in the starting adduct (159.9 pm). With 156.1 pm, the B–N distance at the transition state is close to that of the reactant. In summary, both 1,4- and 1,2-dehydrogenation are mildly endothermic, with $\Delta_{solv}G^0$ values (including solvent effects) next to zero. However, for both pathways significant barriers were found, in agreement to the experimental results (see below), showing that **1** and **2** are stable species at room temperature. The significant difference in the barrier height suggests that 1,4-dehydrogenation is clearly kinetically favoured over 1,2-dehydrogenation for **3** if dehydrogenation is carried out thermally.

Table 1. Thermodynamic properties (ΔE, ΔH^0, ΔG^0, $\Delta_{solv}G^0$ all in kJ mol^{-1}) as calculated for thermal 1,4- and 1,2-dehydrogenation starting with the model guanidine–borane adduct $H_3B{\cdot}N(H)C(NH_2)_2$ (TS = transition state).

	ΔE	ΔH^0	ΔG^0	$\Delta_{solv}G^0$
$H_3B{\cdot}N(H)C(NH_2)_2$ (**3**)	0.0	0.0	0.0	0.0
1,4-Dehydrogenation TS	100.7	86.1	91.5	109.2
$H_2BN(H)C(NH_2)NH + H_2$	48.3	27.5	–6.3	7.0
1,2-dehydrogenation TS	194.1	177.4	179.1	196.5
$H_2BNC(NH_2)_2 + H_2$	43.6	21.6	–15.0	4.1
Isomerisation + 1,4-dehydrogenation				
$HNC(NH_2)(NH_2){\cdot}BH_3$ (**3A**)	56.3	58.7	60.6	65.6
$H_2NC(\mu\text{-}N)(\mu\text{-}NH_2)BH_2 + H_2$	141.6	118.9	86.8	91.1
$H_2BNH_2 + NCNH_2 + H_2$	106.9	72.7	–11.9	–5.7

We also analysed subsequent dimerisation of the diene-type $H_2BN(H)C(NH_2)NH$ and the allene-type $H_2BNC(NH_2)_2$ species to give $[H_2B\{\mu\text{-}N(H)C(NH_2)(NH)\}]_2$ and $[H_2B\{\mu\text{-}NC(NH_2)_2\}]_2$, respectively (see Figure 2 and Table 2). As anticipated, dimerisation of $H_2BN(H)C(NH_2)NH$ (to give an eight-membered ring) comes out to be more exothermic than that of $H_2BNC(NH_2)_2$ (to give a four-membered ring). Interestingly, the calculations predict two conformers of $[H_2B\{\mu\text{-}N(H)C(NH_2)(NH)\}]_2$ ("boat" and "chair") to exhibit almost similar energy. In the solid state, only the chair conformation was found in the case of $[H_2B(\mu\text{-hpp})]_2$ in our experiments (see below). In the case of pyrazabole molecule **4** (see Scheme 1), a boat conformation is adopted, which is (according to B3LYP/6-311+G**) 21.0 kJ mol^{-1} more stable than the chair conformation.[16] Whereas dimerisation to the "boat" conformer of $[H_2B\{\mu\text{-}N(H)C(NH_2)(NH)\}]_2$ is barrier-free (concerning the energy), an energy barrier of 25.0 kJ mol^{-1} (barrier of the free Gibbs energy of 78.1 kJ mol^{-1} at 1 bar, 298 K) has to be surpassed to obtain the dimer of $H_2BNC(NH_2)_2$.

Hydrogen elimination from $[H_2B\{\mu\text{-}N(H)C(NH_2)(NH)\}]_2$ in its "boat" conformer to give the diborane $[HB\{\mu\text{-}N(H)C(NH_2)(NH)\}]_2$ is associated with a change in the standard Gibbs free energy of 25 kJ mol^{-1}. In summary, the calculations on the thermal pathway suggest the first step in the elimination of the first H_2 to be the rate-determining step and predict 1,4-dehydrogenation to be favoured over 1,2-dehydrogenation.

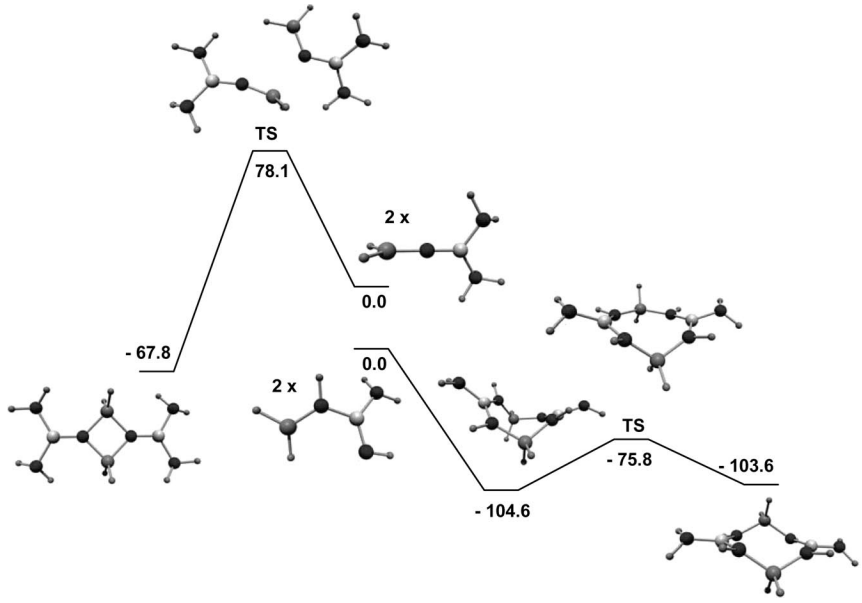

Figure 2. Quantum chemical calculations on the dimerisation of the diene-type $H_2BN(H)C(NH_2)NH$ and the allene-type $H_2BNC(NH_2)_2$ molecules.

Table 2. Thermodynamic properties (ΔE, ΔH^0, ΔG^0, $\Delta_{solv}G^0$ all in kJ mol^{-1}) as calculated for dimerisation of the diene-type $H_2BN(H)C(NH_2)NH$ and the allene-type $H_2BNC(NH_2)_2$ to give $[H_2B\{\mu\text{-}N(H)C(NH_2)(NH)\}]_2$ and $[H_2B\{\mu\text{-}NC(NH_2)_2\}]_2$ (see Figure 2 for a visualisation of the structures).

	ΔE	ΔH^0	ΔG^0	$\Delta_{solv}G^0$
Dimerisation of $H_2BN(H)C(NH_2)NH$ × $H_2BN(H)C(NH_2)NH$	0.0	0.0	0.0	0.0
$[H_2B\{\mu\text{-}N(H)C(NH_2)(NH)\}]_2$ ("boat"-conformation)	–183.9	–171.2	–108.9	–104.6
TS	–154.8	–145.1	–81.3	–75.8
$[H_2B\{\mu\text{-}N(H)C(NH_2)(NH)\}]_2$ ("chair"-conformation)	–182.7	–169.9	–109.0	–103.6
Dimerisation of $[H_2BNC(NH_2)_2]$ × $[H_2BNC(NH_2)_2]$	0.0	0.0	0.0	0.0
TS	25.0	27.6	78.7	78.1
$[H_2B(\mu\text{-}NC(NH_2)_2]_2$	–137.3	–127.4	–68.0	–67.8

All these results are based on the assumption that **3** does not rearrange prior to dehydrogenation. In principal, isomerisation to species **3A** [see Equation (2)] is possible. However, according to quantum chemical calculations, this isomerisation is associated with a change in energy and standard Gibbs free energy (including solvent effects) of 56.3 and 65.6 kJ mol^{-1}, respectively. On the other hand, **3A** is amenable to 1,4-dehydrogenation, which should be associated with a lower activation barrier than that of 1,2-dehydrogenation. Interestingly, the quantum chemical calculations show that this pathway leads to decomposition [see Equation (2)] and formation of H_2BNH_2 (which of course oligomerises directly or after loss of an additional H_2 to give oligomeric amino boranes or imino boranes) and cyanamide ($NCNH_2$). A four-membered ring $H_2NC(\mu\text{-}N)(\mu\text{-}NH_2)BH_2$ is a possible intermediate of this decomposition (see Figure 1). Overall, this pathway is associated with ΔE, ΔH^0, ΔG^0 and $\Delta_{solv}G^0$ values of 50.6, 14.0, –72.4 and –71.3 kJ mol^{-1}, respectively. The corresponding values for reaction to the $H_2NC(\mu\text{-}N)(\mu\text{-}NH_2)BH_2$ intermediate are 85.3, 60.2, 26.2 and 25.5 kJ mol^{-1}, respectively. Unfortunately the activation barrier for this process was not found. We will see in the following section that this route indeed is of importance.

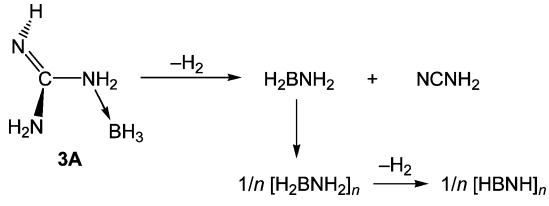

(2)

Catalysed Reaction

The transition states and minima calculated for the Cp_2Ti-catalysed 1,4-dehydrogenation of **3** are illustrated in Figure 3. Table 3 contains the calculated thermodynamic properties. In the first step, Cp_2Ti forms a complex with **3** exhibiting a binding energy of –33.4 kJ mol^{-1}. $\Delta_{solv}G^0$ for complex formation amounts to 32.8 kJ mol^{-1}. The second step is the transfer of the first hydrogen atom from N to Ti and formation of a compound that can in an extreme description be regarded as an ion pair $[Cp_2TiH]^+[H_3B{\cdot}N(H)C(NH)(NH_2)]^-$, but with orbital interactions between the ions and formation of a six-membered TiNCNBH ring. The energy and standard Gibbs free energy (including solvent effects) of this species are –128.8 and –39.0 kJ mol^{-1}, respectively, with respect to the noninteracting reactants Cp_2Ti and **3**. A barrier in the standard solvation Gibbs free energy of 83.4 kJ mol^{-1} (values again relative to free Cp_2Ti and **3**) has to be surpassed. The next step is the conversion of $[Cp_2TiH]^+[H_3B{\cdot}N(H)C(NH)(NH_2)]^-$ into Cp_2TiH_2 and

$H_2BN(H)C(NH_2)NH$. The standard solvation Gibbs free energy barrier of 63.2 kJ mol^{-1} for this step is smaller than that of the previous step. Finally, Cp_2Ti is regenerated and H_2 is released, closing the catalytic cycle. The calculations suggest the rate-determining step to be transfer of the first H atom from the N to the Ti atom, in agreement with the mechanism found for dehydrogenation of $H_3B{\cdot}NHMe_2$.[9]

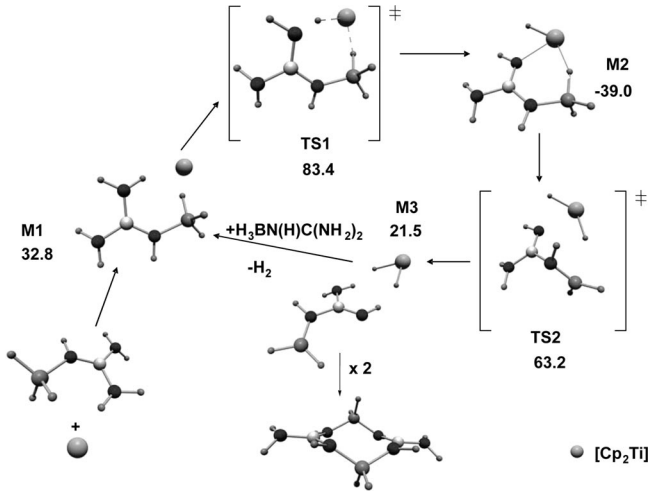

Figure 3. Calculated structures and thermodynamic properties for Cp_2Ti-catalysed 1,4-dehydrogenation of **3**. The solvation free energies ($\Delta_{solv}G$, in kJ mol^{-1}) are relative to [$TiCp_2$] and **3**. The two Cp rings are omitted for clarity.

Table 3. Thermodynamic properties (ΔE, ΔH^0, ΔG^0, $\Delta_{solv}G^0$ all in kJ mol^{-1}) as calculated for 1,4- and 1,2-dehydrogenation starting with the model guanidine–borane adduct $H_3B{\cdot}N(H)C(NH_2)_2$ in the presence of $TiCp_2$ as catalyst (see Figures 3 and 4 for a visualisation of the structures).

	ΔE	ΔH^0	ΔG^0	$\Delta_{solv}G^0$
1,4-Dehydrogenation				
$H_3B{\cdot}N(H)C(NH_2)_2 + TiCp_2$	0.0	0.0	0.0	0.0
M1	–33.4	–28.6	24.4	32.8
TS1	14.6	3.0	65.9	83.4
M2	–128.8	–126.1	–59.0	–39.0
TS2	–21.3	–26.3	40.5	63.2
M3	–33.6	–39.0	4.2	21.5
$H_2BN(H)C(NH_2)(NH) + Cp_2TiH_2$	–17.5	–29.2	–20.2	–13.5
$H_2BN(H)C(NH_2)(NH) + Cp_2Ti + H_2$	48.3	27.5	–6.3	7.0
1,2-Dehydrogenation				
$H_3B{\cdot}N(H)C(NH_2)_2 + TiCp_2$	0.0	0.0	0.0	0.0
M1	–29.2	–23.1	27.6	38.4
TS1	–16.3	–18.8	47.5	64.8
M2	–154.0	–151.7	–83.8	–60.8
TS2	–20.4	–30.8	26.5	45.2
M3	–31.8	–38.9	–2.3	18.9
$H_2BNC(NH_2)_2 + Cp_2TiH_2$	–22.2	–35.1	–28.9	–16.4
$H_2BNC(NH_2)_2 + Cp_2Ti + H_2$	43.6	21.6	–15.0	4.1

The mechanism of Cp_2Ti-catalysed 1,2-dehydrogenation is illustrated in Figure 4. Again, the first step is formation of a complex, this time with a binding energy and standard Gibbs free energy change (including solvent effects) of –29.2 and 38.4 kJ mol^{-1}, respectively. A first solvation Gibbs free energy barrier of 64.8 kJ mol^{-1} relative to the free reactants separates the complex from the Ti intermediate $[Cp_2TiH]^+$-$[H_3BNC(NH_2)_2]^-$. Then, a second solvation Gibbs free energy barrier of 45.2 kJ mol^{-1} has to be surpassed to yield the allene-type species $H_2BNC(NH_2)_2$ and Cp_2TiH_2. In summary, the calculations predict the catalyst to lower significantly the barrier for 1,2-dehydrogenation, whereas the barrier for 1,4-dehydrogenation (which is already relatively small) is only slightly reduced. Under the action of the catalyst, 1,2-dehydrogenation becomes kinetically slightly favoured over 1,4-dehydrogenation.

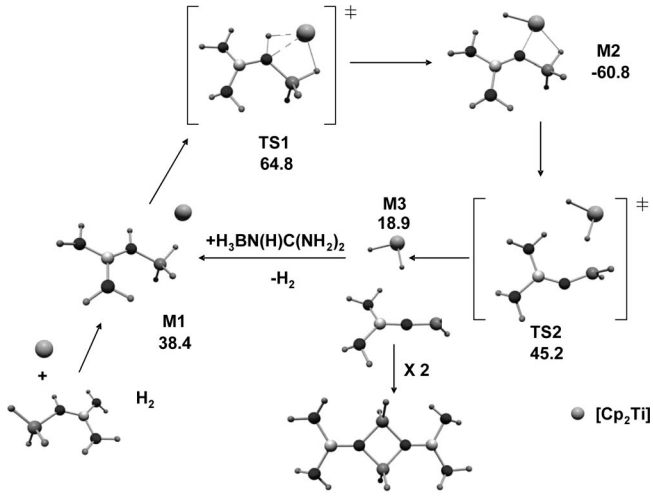

Figure 4. Calculated structures and thermodynamic properties for Cp_2Ti-catalysed 1,2-dehydrogenation of **3**. The solvation free energies ($\Delta_{solv}G$, in kJ mol^{-1}) are relative to [$TiCp_2$] and **3**. The two Cp rings are omitted for clarity.

Experimental Studies

The theoretical results discussed above will be compared in the following to the experimental ones obtained for **1** and **2** (see Scheme 1). For this purpose, we first prepared the two compounds $H_3B{\cdot}$hppH and $H_3B{\cdot}N(H)C(NMe_2)_2$ by reaction between $H_3B{\cdot}NMe_3$ and hppH or $HNC(NMe_2)_2$ as reported previously[11,14] and started the dehydrogenation experiments with a clean toluene solution of one of the guanidine adducts. The reaction products were the same if dehydrogenation was carried out without isolation of the adduct directly from the $H_3B{\cdot}NMe_3$/hppH or $H_3B{\cdot}NMe_3/HNC(NMe_2)_2$ mixtures, but the relative product yields varied slightly. As already mentioned, the two compounds are ideal systems to verify the quantum chemical calculations, as **1** is only amenable to 1,4-dehydrogenation and **2** to 1,2-dehydrogenation. However, **2** could isomerise and is then again amenable to 1,4-dehydrogenation [see Equation (2)].

Uncatalysed Dehydrogenation of $H_3B{\cdot}$hppH (1)

Figure 5 shows ^{11}B NMR spectra recorded before (i) and after thermal treatment (ii: 80 °C, 23 h, iii: 110 °C, 23 h) of a toluene solution of **1**. The ^{11}B NMR spectrum of **1** shows a quartet centred at δ = –19.2 ppm [$^1J(^{11}B,^1H)$ = 93 Hz]. In

both cases of thermal treatment this quartet was extinguished. At the same time, new signals appeared belonging to three different boron products, which are denoted **1A**–**1C** in the following [see Figure 5, Scheme 2, Equations (3) and (4)].

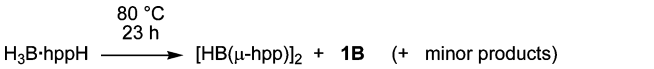

(3)

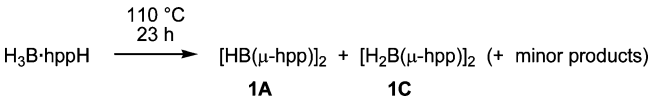

(4)

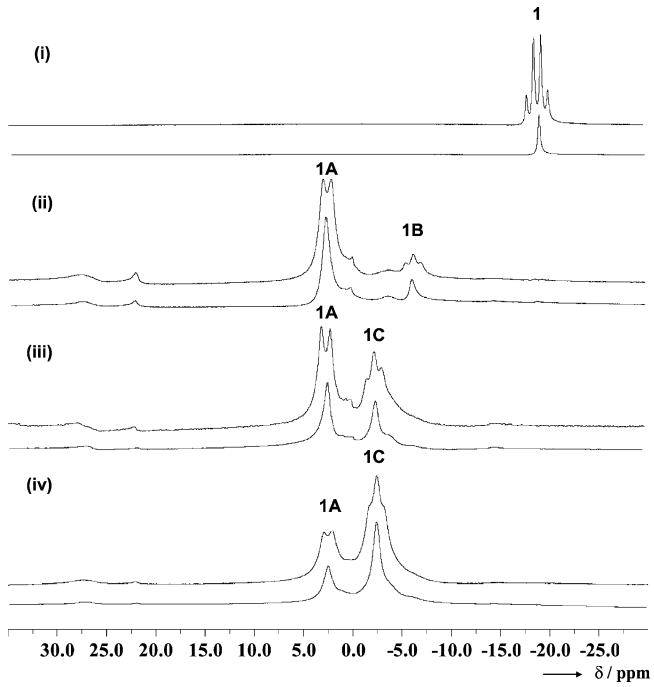

Figure 5. ^{11}B NMR spectra (128.3 MHz) recorded before (i) and after thermal treatment (ii: 80 °C; iii: 110 °C, concentration of **1** in toluene 0.046 mol L^{-1}; iv: 110 °C, concentration of **1** in toluene 0.123 mol L^{-1}) of a toluene solution of **1** for a period of 23 h. The ^{11}B{^{1}H} spectra are also shown underneath each spectrum with coupling allowed.

The reaction at 80 °C led predominantly to species **1A** with a doublet signal centred at δ = 2.5 ppm [$^1J(^{11}B,^1H)$ = 123 Hz]. This species was unambiguously identified as [HB(μ-hpp)]$_2$, and its crystal structure was already reported previously by us.[11,17] The ^{1}H NMR spectrum of this species (see Experimental Section) resembles that of [(Me$_2$HN)B(μ-hpp)]$_2^{2+}$[13] exhibiting a similar rooftop-type structure. A characteristic feature of the ^{1}H NMR spectra of these species is the different chemical shifts of the methylene protons pointing into and away from the roof.[12] In satisfying agreement with the experimental value of $\delta(^{11}B)$ = 2.5 ppm, quantum chemical calculations (see Supporting Information) returned a $\delta(^{11}B)$ value of –3.0 ppm for [HB(μ-hpp)]$_2$. Quantum chemical calculations show that formation of **1A** with release of three equivalents of H$_2$ from two moieties of **1** is associated with a ΔG^0 value (1 bar, 298 K) of –93.8 kJ mol^{-1}. In addition to the doublet from **1A** in the ^{11}B NMR spectrum, a triplet due to a second product **1B** showed at δ = –6.2 ppm. The two most likely candidates for this species are [H$_2$B(κ^{2}N-hpp)] and [H$_2$B(μ-hpp)]$_2$ (see Scheme 2). The latter will be shown to exhibit a different chemical shift. [H$_2$B(κ^{2}N-hpp)] was already previously proposed to be involved in the dehydrogenation reaction,[15] so that we tentatively assigned the triplet signal to [H$_2$B(κ^{2}N-hpp)] (**1B**). Although the hpp ligand generally prefers a bridging (μ^2) coordination, the κ^2 mode is realised in few cases, for example, recently in the Pt^{IV} complex [(κ^2-hpp)(hppH)PtCl$_2$(OAc)].[18] There are also already some structurally characterised guanidinate boron dichlorides known in which the guanidinate is bound in a κ^2-fashion {e.g., [Cy$_2$NC(NCy)$_2$BCl$_2$], [*i*PrNC(NCy)$_2$BCl$_2$][19] or [Ph$_2$NC(NMes$_2$)$_2$BCl$_2$] (Mes = 2,4,6-trimethylphenyl) and [Ph$_2$NC(Ndipp)$_2$BCl$_2$] (dipp = 2,6-*i*Pr$_2$C$_6$H$_3$)}.[20] A calculated chemical shift $\delta(^{11}B)$ of –2.6 ppm for [H$_2$B(κ^{2}N-hpp)] compares with an experimentally observed one of –6.2 ppm. DOSY NMR spectra recorded for the reaction mixture are in line with our tentative assignment. Thus, in toluene the diffusion coefficient for species **1A** measures 5.01·10^{-10} m^2 s^{-1}. By using the Stokes–Einstein equation, a hydrodynamic radius of 623 pm is calculated for this species. Another species with a diffusion coefficient of 7.94·10^{-10} m^2 s^{-1} is also present, corresponding to a radius of 393 pm. Thus, the DOSY experiments indicate that a significantly smaller species is indeed formed.

If the reaction is conducted at 110 °C, the adduct signal also disappeared completely from the ^{11}B NMR spectrum and the doublet signal due to **1A** was seen to grow in. The signal due to **1B** was absent, but a different triplet signal due to a new product **1C** [δ = –2.3 ppm, $^1J(^{11}B,^1H)$ = 96 Hz] appeared instead (see Figure 5). The mixture of compounds was separated by removal of the toluene, addition of hexane and filtration. Compound **1C** turned out to be only sparsely soluble in hexane and formed a precipitate that was after filtration easily redissolved in toluene. The triplet pattern observed in the ^{11}B NMR spectrum (centred at δ = –2.3 ppm, see Figure 5) proved the presence of H$_2$B units. The ^{1}H{^{11}B} NMR spectrum confirmed the presence of hydrogen atoms bound to boron (singlet at δ = 3.51 ppm). Compound **1C** was crystallised from dmso solutions and identified unambiguously as the B^{III} hydride [H$_2$B(μ-hpp)]$_2$. Figure 6 shows the molecular structure according to an X-ray diffraction analysis. Figure 7 displays its NMR spectra and Table 4 includes selected structural parameters. There are two essentially identical crystallographically independent centrosymmetric half molecules in the asymmetric unit. In agreement with the results of quantum chemical calculations (see Supporting Information), the two BH$_2$ groups are located above and below the approximate plane hosting the guanidinate rings thus adopting a chair conformation, and as such, it resembles the structure found previously for [HClGa(μ-hpp)]$_2$.[21] The chemical shift ob-

served in the ^{11}B NMR agrees with that observed for related molecules. For comparison, $\delta(^{11}B)$ = –8.8 ppm and $^{1}J(^{11}B,^{1}H)$ = 108 Hz in the case of compound **4** (see Scheme 1).[22] In difference to **1C**, pyrazabole **4** prefers a boat conformation.[16]

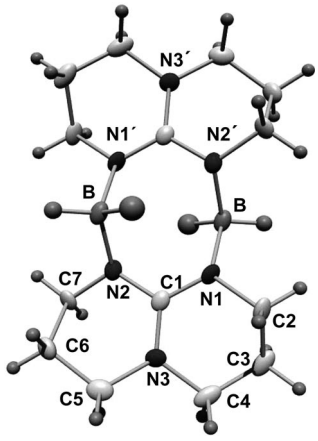

Figure 6. Molecular structure of $[H_2B(\mu\text{-hpp})]_2$ (**1C**). Ellipsoids are drawn at the 50% probability level. Only one of the two independent molecules is shown.

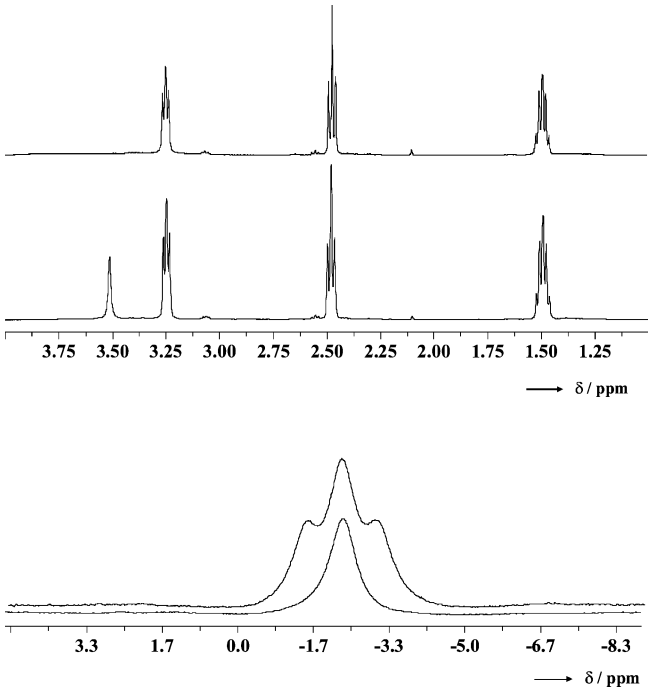

Figure 7. ^{1}H [400 MHz, together with the $^{1}H\{^{11}B\}$ spectrum] and ^{11}B NMR [128.3 MHz, together with the $^{11}B\{^{1}H\}$ NMR] of $[H_2B(\mu\text{-hpp})]_2$ (**1C**).

At first glance it appears counterintuitive that higher temperatures favour the formation of $[H_2B(\mu\text{-hpp})]_2$. The results indeed argue against the formation of $[HB(\mu\text{-hpp})]_2$ by dehydrogenation of $[H_2B(\mu\text{-hpp})]_2$ at 80 °C. Instead, another reaction pathway leading to this species should be favoured at this temperature. To obtain further information, we carried out dehydrogenation experiments

Table 4. Selected bond lengths (in pm) and angles (in °) as measured by X-ray diffraction for the two independent molecules $[H_2B(\mu\text{-hpp})]_2$ (compound **1C**).

B1–N1	156.2(4)/157.8(4)	B1–N2′	156.5(3)/156.4(4)
B1–H1A	116(2)/114(2)	B1–H1B	111(2)/113(2)
C1–N1	135.4(3)/136.2(4)	C1–N2	132.8(4)/131.8(4)
C1–N3	135.9(3)/135.2(4)		
N1–B1–N2′	115.6(2)/116.1(2)	N1–B1–H1A	107(2)/107(2)
N1–B1–H1B	114(2)/109(2)	N1–C1–N2	119.5(2)/118.7(3)
N1–C1–N3	119.5(3)/119.0(3)	N2–C1–N3	121.1(2)/122.3(3)

at 110 °C of toluene solutions with different concentrations of **1**. The spectra obtained for a highly concentrated solution are included in Figure 5(iv). It can be seen that the relative intensities of the signals due to **1A** and **1C** change. Thus, the signal due to **1C** gains intensity relative to that of **1A** for higher concentrations. The fact that the relative product yields alter with the concentration of **1** clearly shows that an intermolecular pathway is followed.

The isolation of $[H_2B(\mu\text{-hpp})]_2$ gives us the opportunity to analyse the conditions for its thermal dehydrogenation. Three experiments were carried out to initiate dehydrogenation of compound **1C**: (a) microwave-assisted dehydrogenation under pressure of a solution of clean $[H_2B(\mu\text{-hpp})]_2$ in toluene at an estimated temperature of 170 °C, (b) thermal

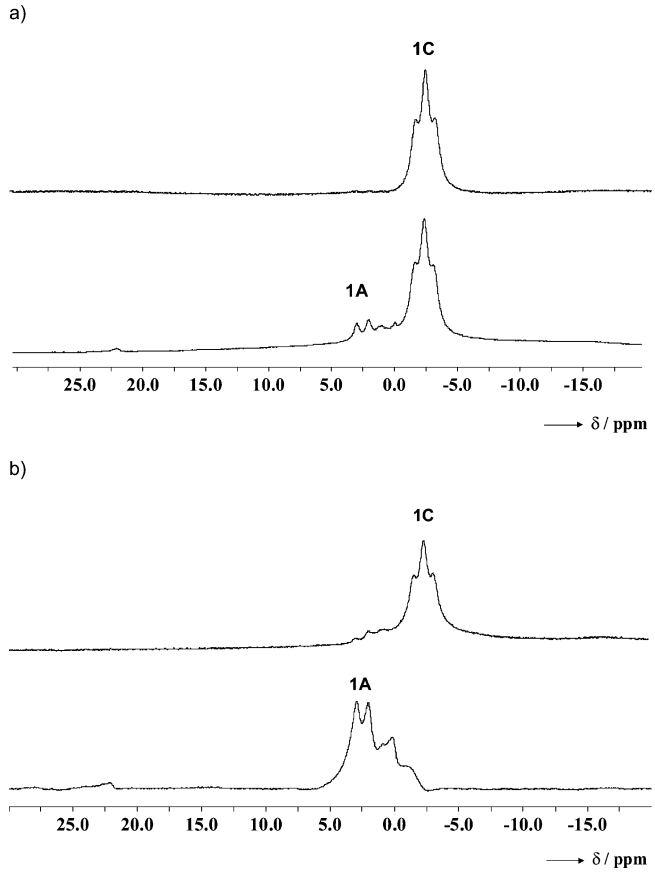

Figure 8. ^{11}B NMR spectra (at 128.3 MHz) in toluene recorded before (upper trace) and after (lower trace) (a) microwave-assisted heating of a toluene solution of **1C** to 170 °C and (b) heating solid **1C** to 200 °C.

dehydrogenation of a solid sample of **1C** at 200 °C and (c) heating of a solution of **1C** in toluene to 110 °C for 6 h. Surprisingly, the spectra recorded for experiment (c) gave no evidence for any reaction product, which indicates that $[H_2B(\mu\text{-hpp})]_2$ is a quite stable species. Figure 8a displays the ^{11}B NMR spectra recorded before and after microwave-assisted dehydrogenation at 170 °C. A small amount of **1A** was formed, but the signal of **1C** still dominated the spectrum. On the other hand, dehydrogenation occurred fast in the solid state at 200 °C (see Figure 8b) with **1A** being the main product. Of course, the reaction mechanism could be different in solution and in the solid phase. In the case of AB and borane adducts to primary and secondary amines it is known that decomposition in the solid state occurs through an intermolecular mechanism that can be explained by the presence of intermolecular N–H···HB dihydrogen bonding.

Uncatalysed Dehydrogenation of $H_3B{\cdot}N(H)C(NMe_2)_2$ (2)

Figure 9 displays the ^{11}B NMR spectra recorded before (i) and after stirring a solution of $H_3B{\cdot}N(H)C(NMe_2)_2$ in toluene for 20 h at 80 °C (ii) and for 6 h to 110 °C (iii). New species **2A** was formed in small amounts [$\delta(^{11}B)$ = –12.6 ppm, q, $^1J(^{11}B,^1H)$ = 98 Hz] in these experiments, but the starting adduct at $\delta(^{11}B)$ = –19.5 ppm [$^1J(^{11}B,^1H)$ = 95 Hz] was still the main component in solution. From the quartet structure of the ^{11}B signal and its position, **2A** can be assigned to a base adduct of BH_3. One possible author of this signal is the isomer of $H_3B{\cdot}N(H)C(NMe_2)_2$, in which one of the N atoms of the amido (NMe_2) groups is bound to boron. Quantum chemical calculations (see Supporting Information) predict this isomer to be less stable by 74.19 kJ mol^{-1} (isomerisation is associated with a change in the Gibbs free energy of 81.76 kJ mol^{-1}) with respect to **2**. As already mentioned, this isomer is amenable to 1,4-elimination. ΔG^0 for this process leading first to H_2BNMe_2 and $NCNMe_2$ [see Equation (5)] is calculated to be –151.4 kJ mol^{-1}.

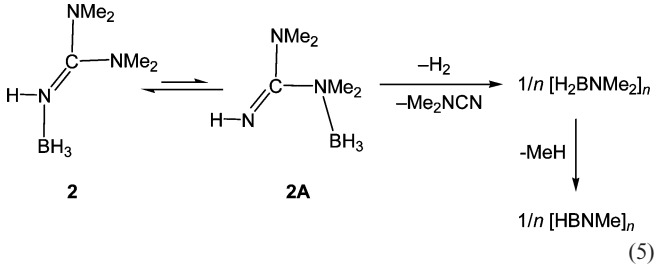

(5)

It is worth mentioning in this context that the Ga analogue of **2**, $H_3GaN(H)C(NMe_2)_2$, was also observed to decompose upon mild heating to give, besides other products, the cluster $HN\{[HGaNMe][H_2GaNC(NMe_2)_2]\}_3GaH$.[23] The [HGaNMe] group within this cluster should arise from such a decomposition pathway. $[H_2GaNC(NMe_2)_2]$ can either stem from 1,2-dehydrogenation of the Ga analogue of **2** or from reaction between H_2GaNMe_2 and $NCNMe_2$. To obtain further information, solutions of **2** were sealed in NMR tubes and heated for 6 d at 80 °C. In the ^{11}B NMR spectrum recorded afterwards [see Figure 9(iv)] the signals of **2** were absent. The spectrum was dominated by a new intense doublet at δ = 29.3 ppm [$^1J(^{11}B,^1H)$ = 128.8 Hz]. This signal can be assigned to oligomeric methylimino borane, $[HBNMe]_n$. For comparison, δ = 31.7 ppm and $^1J(^{11}B,^1H)$ = 130 Hz were reported for trimethyl borazine, $[HBNMe]_3$.[24] In the ^1H NMR spectrum, an intense singlet showed at δ = 2.6 ppm, which is close to the reported value in $[HBNMe]_3$ (δ = 3.0 ppm). Thus, under the applied conditions dihydrogen elimination is a very slow process and leads to decomposition and, upon further methane elimination, formation of oligomeric $[HBNMe]_n$ according to Equation (5). This result is in full agreement with the quantum chemical calculations.

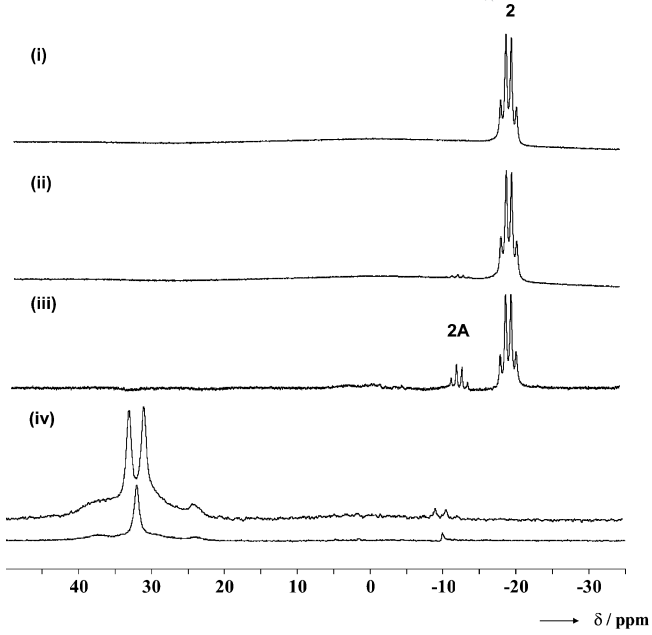

Figure 9. ^{11}B NMR spectrum (at 128.3 MHz) before (i) and after heating a toluene solution of **2** for 20 h to a temperature of 80 °C (ii) and for 6 h to a temperature of 110 °C (iii). Trace (iv) shows the spectrum after dehydrogenation at 80 °C for 6 d in an NMR tube. For (iv) the $^{11}B\{^1H\}$ spectrum is additionally shown.

Catalysed Dehydrogenation of $H_3B{\cdot}hppH$ (1)

In further experiments, dehydrogenation of compounds **1** and **2** was followed in the presence of the potential precatalysts $[Rh(1,5\text{-cod})Cl]_2$ and Cp_2TiCl_2/nBuLi. As mentioned in the introduction, these precatalysts were shown to initiate the room-temperature dehydrogenation of amine boranes;[3,4] the reaction involving the Rh complex is an example of heterogeneous catalysis and that involving the Ti complex is an example of homogeneous catalysis. We present here the results obtained with the Rh catalyst, but the results obtained with Cp_2TiCl_2/nBuLi follow a similar pattern. The appearance of a black metal precipitate signals that the [Rh]-catalysed reaction represents, like that of $H_3B{\cdot}NMe_2H$, a heterogeneous process. A first important result of our studies was that experiments at temperatures below 80 °C showed little change even for prolonged reac-

tion times. In contrast to $H_3B{\cdot}NMe_2H$, for which catalytic dehydrogenation already occurs at room temperature, dehydrogenation of the guanidine–boranes is obviously subjected to a significantly higher barrier even in the presence of a catalyst. NMR spectra were recorded before and after heating a toluene solution of **1** containing the Rh catalyst to a temperature of 80 °C. These experiments showed that reaction in the presence of the catalyst leads at 80 °C predominantly to **1C**, $[H_2B(\mu\text{-hpp})]_2$ [Equation (6)]. This is in clear contrast to the uncatalysed reaction, for which no significant amount of $[H_2B(\mu\text{-hpp})]_2$ was formed under these conditions. The ^1H NMR gave, in addition, evidence for the formation of smaller amounts of species **1F**, which was not observed in the absence of a catalyst.

$$H_3B{\cdot}hppH \xrightarrow[80\ °C,\ 23\ h]{\text{catalyst}} \underset{\mathbf{1C}}{[H_2B(\mu\text{-hpp})]_2} \ (+\ \mathbf{1F}) \qquad (6)$$

In summary the results show that **1C**, $[H_2B(\mu\text{-hpp})]_2$, is formed at 80 °C in the presence of a catalyst, whereas the uncatalysed reaction at 80 °C leads to **1A**, $[HB(\mu\text{-hpp})]_2$, and **1B**, (most likely) $[H_2B(\kappa^2\text{N-hpp})]$. The step-by-step mechanism suggested by the quantum chemical calculations is in line with the experimental results in the case of the catalytic reaction. The uncatalysed dehydrogenation, however, follows a more complicated intermolecular pathway.

Catalysed Dehydrogenation of $H_3B{\cdot}N(H)C(NMe_2)_2$ (2)

The presence of the catalyst has a strong effect on the reaction in the case of the tetramethylguanidine adduct. Dehydrogenation in the absence of a catalyst is an extremely slow process at 80 °C and leads ultimately to decomposition and formation of oligomeric imino borane. In contrast, the catalyst initiates dehydrogenation at 80 °C in much shorter times. This result is in full agreement with the quantum chemical calculations, as now 1,2-dehydrogenation of **2** is possible. Figure 10 displays the ^{11}B NMR spectra before and after heating a toluene solution of **2** for 20 h to 80 °C in the presence of the Rh catalyst. The signals due to **2** disappeared completely. The quartet due to species **2A**, which was also visible in the absence of the catalyst, appeared with weak intensity. Most importantly, the spectrum was dominated by two triplets at δ = –4.4 [$^1J(^{11}B,^1H)$ = 103 Hz] and –1.9 ppm [$^1J(^{11}B,^1H)$ = 101 Hz], which were assigned to boron compounds **2B** and **2C** featuring four-coordinate B atoms. The quantum chemical calculations on **3** suggest that 1,2-dehydrogenation is favoured in the presence of a catalyst, and for **2** only 1,2-dehydrogenation is possible. Therefore, we tentatively assign **2B** to the $HNC(NMe_2)_2$ adduct of $H_2BNC(NMe_2)_2$ and **2C** to the dimer $[H_2B\{\mu\text{-}NC(NMe_2)_2\}]_2$ or the trimer $[H_2B\{\mu\text{-}NC(NMe_2)_2\}]_3$ (see Scheme 3). Dimerisation and trimerisation of $H_2BNC(NMe_2)_2$ according to Equation (7) is associated with an energy change of –102.6 and –137.9 kJ mol^{-1}, respectively. The calculated ^{11}B chemical shifts for **2B** and $[H_2B\{\mu\text{-}NC(NMe_2)_2\}]_2$ are –11.9 and –9.2 ppm, respectively. In addition to these two species a broad feature grew in at δ = ca. 26–28 ppm, which can be assigned to oligomeric and polymeric methylimino boranes. Thus, in the presence of a catalyst 1,2-dehydrogenation indeed becomes favoured over isomerisation and 1,4-dehydrogenation with decomposition into methylimino borane oligomers, in pleasing agreement with the quantum chemical calculations.

$$3\ H_2B{=}N{=}C(NMe_2)_2 \longrightarrow 3/2\ [H_2BNC(NMe_2)_2]_2 \longrightarrow [H_2BNC(NMe_2)_2]_3 \qquad (7)$$

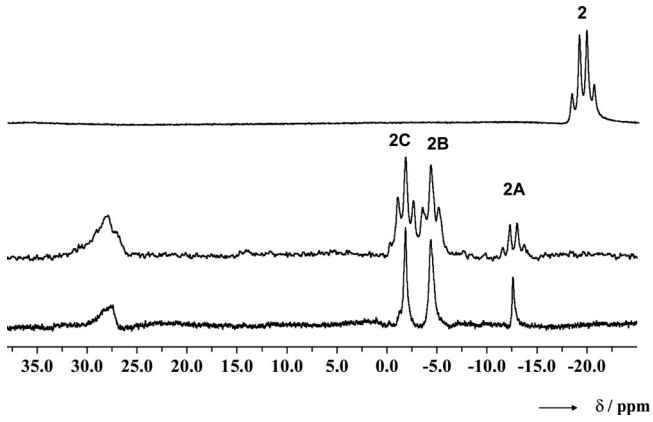

Figure 10. ^{11}B NMR spectrum (at 128.3 MHz) before (upper trace) and after [lower trace, together with the $^{11}B\{^1H\}$ NMR] heating a toluene solution of **2** for 20 h to a temperature of 80 °C in the presence of the Rh catalyst.

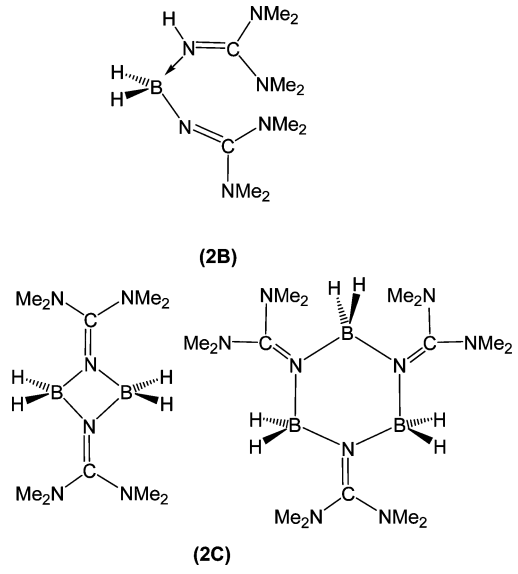

Scheme 3.

Conclusions

In this work the thermal and catalytic dehydrogenation of the two guanidine–borane adducts $H_3B{\cdot}hppH$ (hppH = 1,3,4,6,7,8-hexahydro-2*H*-pyrimido[1,2-*a*]pyrimidine) and $H_3B{\cdot}N(H)C(NMe_2)_2$ were analysed experimentally. In ad-

dition to the experimental work, dehydrogenation was studied by means of quantum chemical calculations for the model complex $H_3B{\cdot}N(H)C(NH_2)_2$. The calculations were built on the assumption of a step-by-step mechanism (shown previously to be favoured in the case of $H_3B{\cdot}NHMe_2$), in which the first products are either the allene-type $H_2BNC(NH_2)_2$ (1,2-dehydrogenation) or the diene-type $H_2BN(H)C(NH_2)(NH)$ (1,4-dehydrogenation), which afterwards dimerise. An alternative route that includes isomerisation of the adduct followed by dehydrogenation and decomposition to give oligomeric amino boranes and imino boranes was also considered.

The calculations clearly showed that the barrier for thermal 1,2-dehydrogenation is much higher than that for 1,4-dehydrogenation arguing for a kinetic preference for 1,4-elimination. Interestingly, the catalyst lowers significantly the barrier for 1,2-dehydrogenation, indicating that the catalyst could alter the preferred reaction channel. The experimental results show that thermal dehydrogenation of guanidine–boranes is a complex process. In the case of $H_3B{\cdot}N(H)C(NMe_2)_2$, dehydrogenation is accompanied by decomposition, leading finally to oligomeric methylimino borane. The calculations suggest that such a reaction is generally preferred for guanidines with hydrogen attached to the imine N atom. Decomposition processes of this kind could open up a new, previously unknown route to borazine and imine borane derivatives. In the case of $H_3B{\cdot}$hppH, thermal dehydrogenation proceeds through an intermolecular mechanism to give the dinuclear species $[H_2B(\mu\text{-hpp})]_2$ and $[HB(\mu\text{-hpp})]_2$, as well as the mononuclear compound $[H_2B(\kappa^2N\text{-hpp})]$. The product distribution depends on the temperature and the concentration. $[H_2B(\mu\text{-hpp})]_2$ turned out to be surprisingly stable and eliminated slowly dihydrogen in solution only at high temperatures under the assistance of microwave treatment, although the reaction is associated with a negative ΔG^0 value. This result implies that the compound is not suitable as a hydrogen transfer reagent. It is a subject of ongoing research in our group to find ways to speed up this process (by modification of the guanidine). The reactions in the presence of a catalyst are in line with the simple "step-by-step" model analysed in the quantum chemical calculations. $H_3B{\cdot}$hppH undergoes catalytic 1,4-dehydrogenation leading to $[H_2B(\mu\text{-hpp})]_2$, and $H_3B{\cdot}N(H)C(NMe_2)_2$ undergoes 1,2-dehydrogenation to give $[H_2BNC(NMe_2)]_n$ (n = 1, 2 or 3). This work provides the basis for future experimental work aiming at the synthesis of oligomeric boron compounds by decomposition of mononuclear guanidine–borane adducts.

Experimental Section

General: Standard Schlenk techniques were applied for all reactions. The solvents were dried and distilled by using standard methods. $H_3B{\cdot}NMe_3$, hppH and 1,1,3,3-tetramethylguanidine were purchased from Sigma–Aldrich and used as delivered. $H_3B{\cdot}$hppH (**1**) and $H_3B{\cdot}N(H)C(NMe_2)_2$ (**2**) were prepared from $H_3B{\cdot}NMe_3$ and hppH or $HNC(NMe_2)_2$ as described previously.[11,14] NMR spectra were measured with a Bruker AVII 400 or a Bruker AVIII-600 spectrometer. Microwave-assisted dehydrogenation experiments were conducted by using a CEM Discover BenchMate (CEM Corp., Matthews, NC). Reactions were performed in 10-mL pressurised vials with "snap-on" caps, which automatically vent the vessel if the internal pressure exceeds 20 bar.

1: ^{1}H NMR (400 MHz, C_6D_6): δ = 6.29 (s, 1 H, NH), 3.34 (t, ^3J = 5.9 Hz, 2 H, H5), 2.83 (br. q, ^1J = 93 Hz, BH), 2.27 (t, ^3J = 5.9 Hz, 2 H, H3), 2.13 (t, ^3J = 6.0 Hz, 2 H, H7), 2.03 (t, ^3J = 6.0 Hz, 2 H, H1), 1.17 (quint, ^3J = 6.0 Hz, 2 H, H6), 0.91 (quint, ^3J = 6.0 Hz, 2 H, H2) ppm. ^{13}C NMR (100.6 MHz, C_6D_6): δ = 150.69 (C4), 47.47 (C5), 47.27 (C7), 46.82 (C1), 38.38 (C3), 21.80 (C6), 21.57 (C2) ppm. ^{11}B NMR (128.3 MHz, C_6D_6): δ = –19.1 [q, ^1J(B,H) = 93 Hz] ppm.

2: ^{1}H NMR (400 MHz, C_6D_6): δ = 4.61 (s, 1 H, NH), 2.80 [br. q, ^1J(B,H) = 95 Hz, 3 H, BH_3], 2.51 (s, 6 H), 1.72 (s, 6 H) ppm. ^{13}C NMR (150.9 MHz, [D$_8$]toluene): δ = 163.88, 39.99, 38.19 ppm. ^{11}B NMR (128.3 MHz, C_6D_6): δ = –19.50 [q, J(B,H) = 95 Hz] ppm. ^{15}N NMR [60 MHz, [D$_8$]toluene, with NH_3(l) as reference]: δ = 116.5 (d, ^1J = 78 Hz, NH), 56.0 (NMe_2), 58.8 (NMe_2) ppm.

Uncatalysed Dehydrogenation of 1 at 80 °C: A solution of $H_3B{\cdot}$hppH (0.15 g, 0.98 mmol) in toluene (10 mL) was stirred for 23 h at 80 °C. Removal of the solvent resulted in an oil, the ^{11}B NMR spectrum of which showed the presence of four products, namely **1A** [δ = 2.5 ppm, d, J(B,H) = 123 Hz] and **1B** [δ = –6.3 ppm, d, J(B,H) = 102 Hz] as well as, in small amounts, **1D** (δ = 22.4 ppm, s) and **1E** (δ = 28.1 ppm, s). Data for $[HB(\mu\text{-hpp})]_2$ (**1A**): ^{1}H NMR (600 MHz, [D$_8$]toluene): δ = 3.43 [ddd, ^2J(H2a,H2b) = 12.5 Hz, ^3J(H2a,H3) = 5.3 Hz, 4 H, H2a], 3.32 [ddd, ^2J(H2b,H2a) = 12.5 Hz, ^3J(H2b,H3) = 4.5 Hz, 4 H, H2b], 2.46 [ddd, ^2J(H4a,H4b) = 11.3 Hz, ^3J(H4a,H3) = 4.5 Hz, 4 H, H4a], 2.36 [ddd, ^2J(H4b,H4a) = 11.3 Hz, ^3J(H4b,H3) = 5.3 Hz, 4 H, H4b] 1.48 (m, 4 H, H3) ppm. ^{13}C NMR (150.92 MHz, [D$_8$]toluene): δ = 47.20 (C4), 45.81 (C2), 23.37 (C3) ppm. ^{11}B NMR (128.30 MHz, [D$_8$]-toluene): δ = 2.5 [d, J(B,H) = 123 Hz] ppm.

Uncatalysed Dehydrogenation of 1 at 110 °C: A solution of $H_3B{\cdot}$hppH (0.071 g, 0.46 mmol) in toluene (10 mL) was stirred for 23 h at 110 °C. Removal of the solvent resulted in an oil, the ^{11}B NMR spectrum of which showed the presence of species **1A** and **1C** and, in small amounts, **1D** and **1E**. Data for $[H_2B(\mu\text{-hpp})]_2$ (**1C**): ^{1}H NMR (400 MHz, C_6D_6): δ = 3.25 [t, ^3J(H2,H3) = 5.8 Hz, 8 H, H2], 2.47 [t, ^3J(H4,H3) = 6.6 Hz, 8 H, H4], 1.49 [quint, ^3J(H3,H2) = 5.8 Hz, ^3J(H3,H4) = 6.6 Hz, 8 H, H3] ppm. ^{13}C NMR (100.56 MHz, C_6D_6): δ = 47.88 (C4), 47.66 (C2), 24.11 (C3) ppm. ^{11}B NMR (128.3 MHz, C_6D_6): δ = –2.4 [t, J(B,H) = 100 Hz] ppm.

Microwave-Assisted Dehydrogenation of $[H_2B(\mu\text{-hpp})]_2$ (1C) at 170 °C: $[H_2B(\mu\text{-hpp})]_2$ (0.06 g, 0.20 mmol) was placed into the microwave vessel and dissolved in toluene (9 mL). The sealed vessel was exposed to microwave irradiation (200 W) for 15 min at a temperature of 170 °C. The ^{11}B NMR spectrum showed mainly unreacted **1C** and the formation of $[HB(\mu\text{-hpp})]_2$ (**1A**) in a small amount.

Dehydrogenation of Solid $[H_2B(\mu\text{-hpp})]_2$ (1C) at 200 °C: A sample of $[H_2B(\mu\text{-hpp})]_2$ (0.08 g, 0.26 mmol) was heated under an Ar atmosphere for 30 min to a temperature of 200 °C. After 15 min of heating the initial solid was converted into an oil. The ^{11}B NMR spectrum indicated the presence of $[HB(\mu\text{-hpp})]_2$ (**1A**) and in small amounts **1D** and **1E**.

Uncatalysed Dehydrogenation of 2 at 80 and 110 °C: A solution of $H_3B{\cdot}N(H)C(NMe_2)_2$ (0.15 g, 1.16 mmol) in toluene (12 mL) was stirred for 20 h at 80 °C. The ^{11}B NMR spectrum recorded after-

wards showed the presence of unreacted $H_3B{\cdot}N(H)C(NMe_2)_2$. In addition, a new weak quartet signal appeared belonging to species **2A** [$\delta(^{11}B)$ = –12.6 ppm, q, J(B,H) = 98 Hz].

Catalysed Dehydrogenation of 1 at 80 °C in the Presence of [Rh(1,5-cod)Cl]$_2$: $H_3B{\cdot}$hppH (0.13 g, 0.80 mmol) was dissolved in toluene (10 mL) and $[Rh(1,5\text{-cod})Cl]_2$ (0.0079 g, 0.016 mmol, ca. 2 mol-% Rh) was added. After stirring the reaction mixture for 23 h at 80 °C, the solution was filtered. The NMR spectra showed the presence of the two species $[H_2B(\mu\text{-hpp})]_2$ (**1C**) and **1F**. Data for **1F**: ^{1}H NMR (400 MHz, C_6D_6): δ = 2.95 (t, ^3J = 5.8 Hz, 2 H, H′2), 2.42 (t, ^3J = 5.8 Hz, 2 H, H′4), 1.36 (quint, ^3J = 5.8 Hz, 2 H, H′3) ppm. ^{13}C NMR (100.6 MHz, C_6D_6): δ = 47.2 (C′4), 41.0 (C′2), 23.0 (C′3) ppm.

Catalysed Dehydrogenation of 2 at 80 °C in the Presence of [Rh(1,5-cod)Cl]$_2$: $H_3B{\cdot}N(H)C(NMe_2)_2$ (0.075 g, 0.58 mmol) was dissolved in toluene (10 mL). $[Rh(1,5\text{-cod})Cl]_2$ (0.0057 g, ca. 2 mol-% Rh) was added as a solid, and the reaction mixture was stirred for 20 h at 80 °C. The solution was filtered, and the pale-yellow solution was concentrated and stored for several weeks at –20 °C. The ^{11}B NMR spectrum provided evidence for the presence of different products **2B** [δ = –4.4 ppm, t, J(B,H) = 106 Hz] and **2C** [δ = –1.9 ppm, t, J(B,H) = 100 Hz]. In addition, weak and broader features showed at δ = 26.9 and 28.2 ppm.

Dehydrogenation of 2 at 80 °C in Sealed NMR Tubes in the Presence of Cp$_2$TiCl$_2$/*n*BuLi: Reaction of $[Cp_2TiCl_2]$ (0.0017 g) in $[D_8]$toluene (0.4 mL) with *n*BuLi (0.009 mL, 1.6 M) in hexane at –10 °C in an NMR tube resulted in the formation of a red-brown solution in 3 min. After being warmed to room temperature, **2** (0.04 g, 0.31 mmol) in $[D_8]$toluene (0.6 mL) was added, and the reaction mixture was stirred for 3 min in an ultrasonic bath, which resulted in a change of colour from red-brown to grey. After flame sealing the NMR tube, the reaction was heated for ca. 6 d at 80 °C. The reaction was monitored by NMR spectroscopy by providing evidence for the formation of **2B** and **2C** as well as two further products with ^{11}B signals at δ = 26.9 and 28.2 ppm.

X-ray Crystal Structure Structure Determination: Crystal data and details of the structure determination are listed in Table 5. Intensity data were collected at 100(2) K with a Bruker AXS Smart 1000 CCD diffractometer (Mo-K_α radiation, graphite monochromator, λ = 0.71073 Å). Data were corrected for Lorentz, polarisation and absorption effects (semiempirical, SADABS).[25] All of several crystals examined appeared to belong to the orthorhombic crystal system, apparent space group *Pbca*. Close inspection of the data at high Bragg angles, however, revealed the presence of pseudo-merohedral twinning, with two monoclinic individuals related by a twofold twin axis along their common cell vector *b* [refined fractional contributions of the two twin domains 0.508(4), 0.492(4)]. After assignment of the correct space group $P2_1/c$ the structure could be solved by direct methods with dual-space recycling ("Shake-and-Bake")[26] and was refined by full-matrix least-squares methods based on F^2 against all reflections.[27] All non-hydrogen atoms were given anisotropic displacement parameters. The hydrogen atoms of the methylene groups were input at calculated positions and refined with a riding model. The hydrogen atoms on boron were taken from difference Fourier syntheses and refined with separate similarity restraints for the two types of B–H bonds. CCDC-690038 contains the supplementary crystallographic data for this paper. These data can be obtained free of charge from The Cambridge Crystallographic Data Centre via www.ccdc.cam.ac.uk/data_request/cif.

Table 5. Crystal data and refinement details of $[H_2B(\mu\text{-hpp})]_2$ (compound **1C**).

Formula	$C_{14}H_{28}B_2N_6$
M_r [g mol^{-1}]	302.04
Crystal size [mm]	0.25 × 0.13 × 0.10
Crystal system	monoclinic
Space group	$P2_1/c$
a [Å]	8.0912(4)
b [Å]	12.6485(7)
c [Å]	15.5315(8)
β [°]	90.1630(10)
V [Å^3]	1589.51(14)
$\rho_{calcd.}$ [g cm^{-3}]	1.262
Z	4
F(000)	656
Range *hkl* (indep. set)	–11 to 11, 0 to 18, 0 to 22
θ range [°]	1.3–31.5
μ [mm^{-1}]	0.078
T_{max}/T_{min}	0.8623/0.7974
Measured reflections	39130 [0.0398]
Unique reflections [R_{int}]	5255
Observed reflections [$I > 2\sigma(I)$]	4092
Refined parameters/restraints	216/2
Goodness-of-fit	1.08
$R(F)$ [$F_o > 4\sigma(F_o)$]	0.0559
$wR(F^2)$ (all data)	0.1451
Residual electron density [e Å^{-3}]	0.388/–0.285

Calculation Details: All calculations were carried out with the Gaussian 03 program package.[28] For the mechanistic calculations on **3** we used the B3LYP density functional. We chose for all guanidine atoms a 6-31++G**, for Ti a LANL2DZ and for the atoms of the Cp rings a 6-31G* basis set. This level has proved its efficiency on a similar system[9] and allowed us to obtain results in a reasonable time. It was particularly useful in the research of the transitions states. All the thermodynamic properties calculations are carried on at standard conditions. The solvation effects on electronic energies were estimated on all structures optimised in gas phase by using the CPCM model.[29] The $\Delta_{solv}G°$ values are based on the gas-phase values to which we added the contribution of the solvation effect on the electronic energies. The energy-minimum structures and the $\delta(^{11}B)$ chemical shifts of all other compounds discussed in this work (see structures and chemical shifts in the Supporting Information) were calculated at the DFT-GIAO//B3LYP/6-311+G* level. All calculated $\delta(^{11}B)$ chemical shifts were (like the experimental ones) referenced to $F_3B{\cdot}OEt_2$.

Supporting Information (see footnote on the first page of this article): ^{1}H NMR (400 MHz, C_6D_6) spectrum of **1** and **2**; ^{1}H–^{15}N correlated NMR spectrum of **2**; structural parameters for the transition states and minima of the 1,2- and 1,4-dehydrogenation of **3**; calculated structures and ^{11}B NMR chemical shifts of possible dehydrogenation products of **1** and **2**; coordinates calculated for the thermal and catalytic dehydrogenation of **3**.

Acknowledgments

The authors gratefully acknowledge financial support by the Deutsche Forschungsgemeinschaft. We thank Klaus Hempel for helping us with the microwave experiments.

[1] See, for example: a) F. H. Stephens, V. Pons, R. T. Baker, *Dalton Trans.* **2007**, 2613–2626; b) T. B. Marder, *Angew. Chem.*

2007, *119*, 8262–8264; *Angew. Chem. Int. Ed.* **2007**, *46*, 8116–8118; and references given therein.
[2] a) C. A. Jaska, A. Bartole-Scott, I. Manners, *Dalton Trans.* **2003**, *21*, 4015–4021; b) T. J. Clark, K. Lee, I. Manners, *Chem. Eur. J.* **2006**, *12*, 8634–8648; and references given therein.
[3] a) C. A. Jaska, K. Temple, A. J. Lough, I. Manners, *J. Am. Chem. Soc.* **2003**, *125*, 9424–9434; b) C. A. Jaska, I. Manners, *J. Am. Chem. Soc.* **2004**, *126*, 9776–9785.
[4] M. C. Denney, V. Pons, T. J. Hebden, D. M. Heinekey, K. I. Goldberg, *J. Am. Chem. Soc.* **2006**, *128*, 12048–12049.
[5] J.-M. Yan, X.-B. Zhang, S. Han, H. Shioyama, Q. Xu, *Angew. Chem.* **2008**, *120*, 2319–2321; *Angew. Chem. Int. Ed.* **2008**, *47*, 2287–2289.
[6] J. X. McDermott, M. E. Wilson, G. M. Whitesides, *J. Am. Chem. Soc.* **1976**, *98*, 6529.
[7] T. J. Clark, C. A. Russell, I. Manners, *J. Am. Chem. Soc.* **2006**, *128*, 9582–9583.
[8] J. L. Fulton, J. C. Linehan, T. Autrey, M. Balasubramanian, Y. Chen, N. K. Szymczak, *J. Am. Chem. Soc.* **2007**, *129*, 11936–11949.
[9] Y. Luo, K. Ohno, *Organometallics* **2007**, *26*, 3597–3600.
[10] F. H. Stephens, R. T. Baker, M. H. Matus, D. J. Grant, D. A. Dixon, *Angew. Chem.* **2007**, *119*, 760–763; *Angew. Chem. Int. Ed.* **2007**, *46*, 746–749.
[11] O. Ciobanu, P. Roquette, S. Leingang, H. Wadepohl, J. Mautz, H.-J. Himmel, *Eur. J. Inorg. Chem.* **2007**, 4530–4534.
[12] O. Ciobanu, D. Emeljanenko, E. Kaifer, H.-J. Himmel, *Inorg. Chem.* **2008**, *47*, 4774–4778.
[13] R. Dinda, O. Ciobanu, H. Wadepohl, O. Hübner, R. Acharraya, H.-J. Himmel, *Angew. Chem.* **2007**, *119*, 9270–9273; *Angew. Chem. Int. Ed.* **2007**, *46*, 9110–9113.
[14] O. Ciobanu, S. Leingang, H. Wadepohl, H.-J. Himmel, *Eur. J. Inorg. Chem.* **2008**, 322–329.
[15] O. Ciobanu, H.-J. Himmel, *Eur. J. Inorg. Chem.* **2007**, 3565–3572.
[16] E. Cavero, R. Giménez, S. Uriel, E. Beltrán, J. L. Serrano, I. Alkorta, J. Elguero, *Cryst. Growth Des.* **2008**, *8*, 838–847.
[17] In the previous work, the presence of two species in the NMR spectra was reported. These two species were assigned to different isomers of $H_2B_2(hpp)_2$. However, in light of our new results, we have to reassign the signals.
[18] A. Peters, U. Wild, O. Hübner, E. Kaifer, H.-J. Himmel, *Chem. Eur. J.* **2008**, *14*, 7813–7821.
[19] G. A. Pierce, N. D. Coombs, D. J. Willock, J. K. Day, A. Stasch, S. Aldridge, *Dalton Trans.* **2007**, 4405.
[20] M. Findlater, N. J. Hill, A. H. Cowley, *Dalton Trans.* **2008**, 4419–4423.
[21] G. Robinson, C. Y. Tang, R. Köppe, A. R. Cowley, H.-J. Himmel, *Chem. Eur. J.* **2007**, *13*, 2648–2654.
[22] S. Trofimenko, *J. Am. Chem. Soc.* **1966**, *88*, 1842–1844.
[23] A. R. Cowley, A. J. Downs, H.-J. Himmel, S. Marchant, S. Parsons, J. A. Yeoman, *Dalton Trans.* **2005**, 1591–1597.
[24] O. T. Beachley Jr., *Inorg. Chem.* **1969**, *8*, 981–985.
[25] G. M. Sheldrick, *SADABS*, Bruker AXS, **2004**–**2008**.
[26] *SIR2004*, CNRIC, Bari, Italy, **2004**; M. C. Burla, R. Caliandro, M. Camalli, B. Carrozzini, G. L. Cascarano, L. De Caro, C. Giacovazzo, G. Polidori, R. Spagna, *J. Appl. Crystallogr.* **2005**, *38*, 381.
[27] G. M. Sheldrick, *SHELXL-97*, University of Göttingen, **1997**; G. M. Sheldrick, *Acta Crystallogr., Sect. A* **2008**, *64*, 112.
[28] M. J. Frisch, G. W. Trucks, H. B. Schlegel, G. E. Scuseria, M. A. Robb, J. R. Cheeseman, V. G. Zakrzewski, J. A. Montgomery Jr., R. E. Stratmann, J. C. Burant, S. Dapprich, J. M. Millam, A. D. Daniels, K. N. Kudin, M. C. Strain, O. Farkas, J. Tomasi, V. Barone, M. Cossi, R. Cammi, B. Mennucci, C. Pomelli, C. Adamo, S. Clifford, J. Ochterski, G. A. Petersson, P. Y. Ayala, Q. Cui, K. Morokuma, D. K. Malick, A. D. Rabuck, K. Raghavachari, J. B. Foresman, J. Cioslowski, J. V. Ortiz, B. B. Stefanov, G. Liu, A. Liashenko, P. Piskorz, I. Komaromi, R. Gomperts, R. L. Martin, D. J. Fox, T. Keith, M. A. Al-Laham, C. Y. Peng, A. Nanayakkara, C. Gonzalez, M. Challacombe, P. M. W. Gill, B. Johnson, W. Chen, M. W. Wong, J. L. Andres, C. Gonzalez, M. Head-Gordon, E. S. Replogle, J. A. Pople, *Gaussian 03*, Gaussian Inc., Pittsburgh, PA **1998**.
[29] a) V. Barone, M. Cossi, *J. Phys. Chem. A* **1998**, *102*, 1995–2001; b) M. Cossi, N. Rega, G. Scalmani, V. Barone, *J. Comput. Chem.* **2003**, *24*, 669–681.

Received: June 4, 2008
Published Online: November 5, 2008

